LANGMUIR Article
Cite This: Langmuir 2019, 35, 4020−4028
pubs.acs.org/Langmuir

Tracing Size and Surface Chemistry-Dependent Endosomal Uptake of Gold Nanoparticles Using Surface-Enhanced Raman Scattering

Deniz Yaşar Öztaş,[†] Mine Altunbek,[†] Deniz Uzunoglu,[†] Hülya Yılmaz,[†] Demet Çetin,[‡] Zekiye Suludere,[§] and Mustafa Çulha*[,†]

[†]Department of Genetics and Bioengineering, Faculty of Engineering, Yeditepe University, Ataşehir, Istanbul 34755, Turkey
[‡]Department of Mathematics and Science Education, Gazi Faculty of Education and [§]Department of Biology, Faculty of Science, Gazi University, Ankara 06500, Turkey

Supporting Information

ABSTRACT: Surface-enhanced Raman scattering (SERS)-based single-cell analysis is an emerging approach to obtain molecular level information from molecular dynamics in a living cell. In this study, endosomal biochemical dynamics was investigated based on size and surface chemistry-dependent uptake of gold nanoparticles (AuNPs) on single cells over time using SERS. MDA-MB-231 breast cancer cells were exposed to 13 and 50 nm AuNPs and their polyadenine oligonucleotide-modified forms by controlling the order and combination of AuNPs. The average spectra obtained from 20 single cells were analyzed to study the nature of the biochemical species or processes taking place on the AuNP surfaces. The spectral changes, especially from proteins and lipids of endosomal vesicles, were observed depending on the size, surface chemistry, and combination as well as the duration of the AuNP treatment. The results demonstrate that SERS spectra are sensitive to trace biochemical changes not only the size, surface chemistry, and aggregation status of AuNPs but also the endosomal maturation steps over time, which can be simple and fast way for understanding the AuNP behavior in single cell and useful for the assisting and controlling of AuNP-based gene or drug delivery applications.

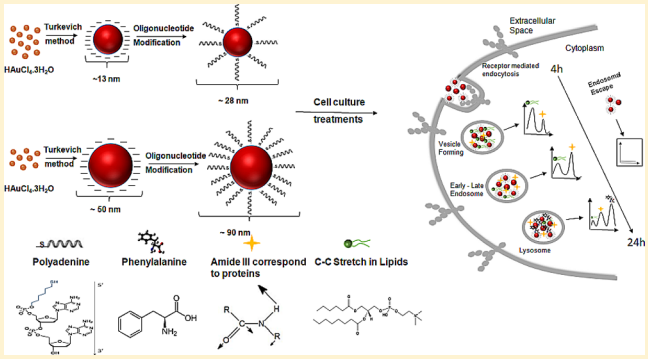

INTRODUCTION

In a cell population, each cell exhibits distinct variations at biomolecular level.[1] In the analysis of a large heterogeneous population, major characteristics of cells may mask the minor characteristics of abnormalities.[2] To overcome this limitation, single-cell analysis, where molecular information can be collected at the individual cell level, has emerged in many fields such as biomedical research and cancer biology. Several single-cell analysis approaches such as comet assay,[3] DNA sequencing,[4] single-cell PCR,[5] flow cytometry,[6] and mass spectrometry[7] were developed. Other techniques including atomic force microscopy[8] and fluorescence microscopy[9] are still being evaluated for the goal.

Raman spectroscopy (RS) is a unique vibrational spectroscopic technique, which has been investigated for single-cell analysis since 1990.[10] RS can provide molecular level information about the chemical nature of a cell without any labeling or staining procedure.[11] In the first reports of RS, cell fixation procedures were performed to monitor the proteins, lipids, and mitochondria.[12] However, it was shown that fixation might cause spectral changes for molecular characteristics.[13] Following the mentioned study, the cell fixation procedure was no longer used for cellular studies and RS was performed without any fixation.[14,15] However, RS has one main disadvantage: inherently weak signals.[16] To overcome this problem, a variant of RS, surface-enhanced Raman scattering (SERS), was developed.[17] The first single-cell analysis using SERS was reported in 1991 by Nabiev et al.,[18] and in recent years, there has been a growing interest in using SERS for single-cell analysis. Some examples of SERS being performed at the single-cell level are detection of biomarker molecules,[19] glucose,[20] investigation of cell response to nanomaterials,[21] cell differentiation, and cell cycle phases.[22,23]

In this technique, noble metal (gold or silver) nanosubstrates are used to enhance the Raman scattering.[24,25] In order not to disturb the cell integrity for living cell analysis, the use of nanosubstrates requires special attention during living cell SERS analysis. Currently, both noncolloidal and colloidal substrates are being heavily investigated for their suitability in living cell SERS applications. In the case of noncolloidal substrate-based approaches, sensitive and reproducible SERS spectra were obtained from cell membrane, mitochondria, and inner cell components such as DNA/RNA in the nucleus.[26−31] However, the remaining contaminants on the substrate

Received: November 29, 2018
Revised: February 13, 2019
Published: February 18, 2019

Downloaded via SABANCI UNIV on December 25, 2020 at 10:43:01 (UTC).
See https://pubs.acs.org/sharingguidelines for options on how to legitimately share published articles.

© 2019 American Chemical Society

DOI: 10.1021/acs.langmuir.8b03988
Langmuir 2019, 35, 4020−4028

surfaces increase the susceptibility to spectrum overlapping with the other cell components. This can limit the reliability of the technique.

The use of colloidal-based substrates might provide more reliable intracellular information. For this, it is important to get the plasmonic NPs aggregated in intracellular locations for SERS analysis. NPs are mostly incorporated into living cells through endocytosis, by simply adding NPs into the serum media without applying any mechanical force. Other physical approaches such as electroporation or microinjection are also used to effectively aggregate nanoparticles. However, these can easily damage cells.[32−34]

Because of their nontoxicity, gold nanoparticles (AuNPs) are known to be a more suitable substrate for living cell SERS analysis.[35] It is now clear that the delivery of AuNPs into cells through endocytosis changes based on their size, shape, and surface chemistry.[36] Because the cellular uptake and dependently intracellular aggregation affect the plasmonic properties of NPs, SERS activity dependently changes. It was reported that an average of 50 nm spherical NPs is more effectively taken up into the cells.[37] Coincidentally, the aggregates formed by AuNPs with 50 nm average size are also desired for the improved SERS enhancement.[38,39]

Endocytosis is an energy-dependent process associated with various intracellular biochemical processes. Any abnormality, disease, or any homeostatic process such as nutrient uptake or apoptosis can affect the dynamic biochemical processes of endocytosis. A carefulinvestigation can help to understand the endocytosis of newly emerged targeted agents and to assist and control the biological responses for specific diseases. Thus, tracing the biochemical processes of endocytosis with the aid of AuNPs entrapped in endosomal vesicles can lead to the discovery of new functional therapeutic approaches in cancer therapy, especially for metastasis, in a simple and fast way.

Since the amount of uptake and aggregation of AuNPs plays a pivotal role for the enhancement of SERS scattering in single-cell analysis, concentration and exposure time of AuNPs are important factors for spectral outcomes. Kneipp's group was the first to report the use of AuNPs in SERS single living cell analysis.[40] In a later study, the same group conducted a series of experiments to monitor biochemical changes around AuNPs over time.[41] They showed that SERS signals from cells could be obtained as early as 10−20 min of incubation of cells with AuNPs. They have also showed that the spectra changed drastically among different cell lines and over time with the formation of aggregates. These observations demonstrate the feasibility and sensitivity of SERS for intracellular applications. Huefner et al. focused on the biochemical processes in endosomes during the maturation from early to late endosomes by simply applying a pulse/depletion method in another study.[42] In their method, two groups of AuNP-treated cells were used for the evaluation. Before the SERS measurement, the first group of cells was incubated with AuNPs for 48 h (pulse), and then for an additional 24 h in a fresh medium (depletion), whereas the second group was incubated with AuNPs for 72 h. The spectra from the former were used to interpret the biochemical changes in late endosomes, whereas the latter ones were used for the biochemical changes in early endosomes.

Because the increased uptake and aggregation are desired to obtain effective SERS signals, gold (Au−magnetite) and silver nanoparticles (Ag−magnetite) linked with magnetite particles were used to increase the intracellular uptake and aggregation with the aid of a magnetite in another study.[43] It was demonstrated that, compared to pure AuNPs and AgNPs, the uptake of Au−magnetite and Ag−magnetite into the cells increased by two- to threefolds. However, the spectra obtained from Au−magnetite and Ag−magnetite behaved differently from the pure AuNP and AgNPs. This was due to the different adsorptions of biomolecules on different composite nanostructures. In another study, Mahajan's group demonstrated that even though it was not visible on the cell viability results, the increased uptake could perturb the intracellular functions.[44] As seen, these parameters play an important role in cellular functions, spectral outcome, and SERS signal quality. Therefore, the concentration and incubation time of particles should be carefully considered while evaluating the other variables such as surface chemistry.

In our previous study, using a reporter-free SERS methodology, we evaluated the cytotoxicity of nanomaterials. We have simply added 50 nm AuNPs as a SERS substrate and then the nanoparticles such as ZnO, TiO_2, NPs, and single-walled carbon nanotubes into the cell culture medium before the SERS measurements. Then, the obtained SERS spectra was used form the cytotoxicity assesment.[21] In this current study, we have used SERS to investigate the biochemical changes during endocytosis of the AuNPs with different sizes and surface chemistries over time. The AuNPs with 50 nm ($AuNPs_{50}$) and 13 nm ($AuNPs_{13}$) average particle sizes and their polyadenine oligonucleotide-modified forms ($AuNPs_{50}$-oligo and $AuNPs_{13}$-oligo, respectively) were used for the investigation. Basically, $AuNPs_{50}$ was used as a SERS substrate and with their potential in drug or gene delivery applications, the polyadenine oligonucleotide-modified AuNPs were used as a model to evaluate the surface chemistry-dependent biochemical changes during endocytosis.[45] The endosomal activity was traced systematically by controlling the order and combination of AuNPs treatment. The AuNPs were simply introduced into the medium of MDA-MB-231 breast cancer cell line and incubated for 4, 8, 12, and 24 h. The localization and aggregation of the AuNPs inside the cells were monitored using transmission electron microscopy (TEM). The biochemical processes during endocytosis were analyzed using SERS at the single-cell level without any labeling or staining procedure.

EXPERIMENTAL SECTION

Synthesis and Modification of AuNPs. Gold(III) chloride trihydrate ($HAuCl_4{\cdot}3H_2O$) was purchased from Sigma-Aldrich (USA), and trisodium citrate dihydrate ($C_6H_5Na_3O_7{\cdot}2H_2O$) was purchased from Merck (Germany). Two different sizes of AuNPs with an average of 13 nm ($AuNPs_{13}$) and 50 nm ($AuNPs_{50}$) were synthesized using the Turkevich Method.[46] For the synthesis of $AuNPs_{13}$, 40 mg of gold chloride ($HAuCl_4{\cdot}3H_2O$) and for the synthesis of $AuNPs_{50}$, 10 mg of $HAuCl_4{\cdot}3H_2O$ was first dissolved in 100 mL of ddH_2O. The solutions were heated under stirring until boiling. Then, for the synthesis of $AuNPs_{13}$, 10 mL of 38.8 mM sodium citrate ($Na_3C_6H_5O_7$) solution and, for the synthesis of $AuNPs_{50}$, 1 mL of 1% $Na_3C_6H_5O_7$ solution were added to the boiling solutions very quickly. The solutions were boiled for 15 min and left at room temperature for cooling.

For the modification of AuNPs, polyadenine oligonucleotides were purchased from Alpha DNA (Canada). Both of the AuNPs were modified with oligonucleotides by using the salt aging procedure.[47] First, phosphate buffer was prepared using potassium phosphate monobasic (KH_2PO_4) (Merck, Germany) and potassium phosphate dibasic (K_2HPO_4) (Sigma-Aldrich, USA). Briefly, 100 μL of 0.1 M phosphate buffer and 100 μL of 0.1% sodium dodecyl sulfate

DOI: 10.1021/acs.langmuir.8b03988
Langmuir 2019, 35, 4020−4028

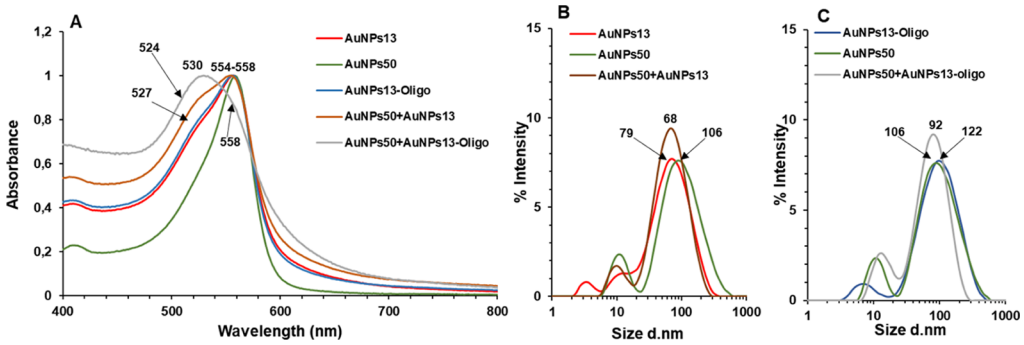

Figure 1. UV/vis (A) and DLS (B,C) spectra of colloidal suspension of $AuNPs_{13}$, $AuNPs_{50}$, $AuNPs_{13}$-oligo, $AuNPs_{50}$ + $AuNPs_{13}$, and $AuNPs_{50}$ + $AuNPs_{13}$-oligo in the cell culture medium.

($C_{12}H_{25}O_4SNa$) (Bio Basic Inc., Canada) were added into 1 mL of $AuNPs_{13}$ and $AuNPs_{50}$, respectively. A 20 μL of 100 μM 3′-thiol modified 20-mer polyadenine oligonucleotide (3′-SH-AAAAAAAAAAAAAAAAAAAA) was added into the $AuNPs_{13}$ suspension, whereas 30 μL of oligonucleotide was added to $AuNPs_{50}$ suspension. Both of the suspensions were mixed gently for 30 min at room temperature. After mixing, 100 μL of 2 M sodium chloride (NaCl) (Sigma-Aldrich, USA) solution was added into prepared suspensions in three steps. After every step, the suspensions were sonicated for 20 s and mixed gently for 30 min. After the last step, the suspensions were incubated overnight, under gently mixing. To remove excess oligonucleotides, suspensions were centrifuged at 13 000 rpm for 20 min and the pellet was resuspended with ddH_2O. This step was repeated three times.

Characterization of AuNPs. The absorbance of 13 nm AuNPs, 50 nm AuNPs, and AuNPs-oligo was measured using a UV/vis spectrometer (PerkinElmer, USA). Hydrodynamic sizes were measured using Zetasizer Nano-ZS (Malvern, UK) at a 173° scattering angle with a 4 mW He−Ne laser at room temperature. The prepared samples were placed into polystyrene cuvettes for the measurements. The refractive index and absorption of the AuNPs were set as 2.0 and 0.320, respectively. The measurements were repeated three times.

Cell Culture Experiments. MDA-MB-231 breast cancer cell line was purchased from American Type Culture Collection (USA). MDA-MB-231 cells were cultured in high-glucose Dulbecco's modified Eagle's medium (DMEM) (Gibco, USA) containing 10% fetal bovine serum (FBS) and 1% PS at 37 °C under 5% CO_2 humidified atmosphere. Cells were passaged and seeded again every 3−4 days.

For the investigation of protein corona formation and the interaction of AuNPs in their-mixture of treatments and their aggregation, the AuNPs were suspended in DMEM containing 10% FBS and 1% PS based on the treatment concentrations described below. After the incubation in an incubator at 37 °C with increasing incubation times (0, 1, 2, and 4 h), the samples were analyzed by using UV/vis spectroscopy and dynamic light scattering (DLS).

For SERS measurements, MDA-MB-231 cells were seeded in 24-well plates at the density of 20 000 cells/well and incubated for 24 h for attachment. After 24 h, cells were treated with 25 nM of $AuNPs_{50}$ and $AuNPs_{50}$-oligo as determined in our previous study.[21] For mixture treatments, cells were incubated together with 25 nM $AuNPs_{50}$ + 10 nM $AuNPs_{13}$ and 25 nM $AuNPs_{50}$ + 10 nM $AuNPs_{13}$-oligo. Schematic representation of experimental setup is shown in Figure S6.

For investigation of cytotoxicity of NPs, the WST-1 assay was used (Roche, USA). MDA-MB-231 cells were seeded in 96-well plates at the density of 5000 cells/well and incubated for 24 h for attachment. After incubation, cells were treated with $AuNPs_{13}$, $AuNPs_{13}$-oligo, $AuNPs_{50}$, $AuNPs_{50}$-oligo, mixture of $AuNPs_{50}$ and $AuNPs_{13}$, and mixture of $AuNPs_{50}$ and $AuNPs_{13}$-oligo at concentrations of 2.5, 5, 10, 15, 20, and 25 nM for 24 h. Then, cells were incubated with a fresh cell culture medium containing 10% WST-1 dye for 1.5 h. Cell viability was measured by using a microplate reader ELx800 Absorbance Reader (Biotek, USA) at 450 nm.

TEM Imaging. MDA-MB-231 cells were washed with 1× phosphate-buffered saline (PBS) and collected using a cell scraper. Gluteraldehyde (2.5%) was used to prefix the collected cells. Then, the cells were washed with PBS, again. For the post fixation step, 1% OsO_4 solution at 4 °C was used. The OsO_4 solution was removed, and cells were rinsed with buffer. Centrifugation was performed, and then low melting agarose was poured onto the culture's pellets. The samples were cooled, solidified, dehydrated in ethanol, placed in propylene oxide, and embedded in araldite. Araldite blocks were cut using the Leica EM UC6 Ultramicrotome, and these sections were stained with lead citrate and uranyl acetate. Images of the samples were collected by using a JEOL JEM 1400 Transmission Electron Microscope at an accelerating voltage of 80 kV.

SERS Measurements. After 4, 8, 12, and 24 h incubation with the AuNPs, MDA-MB-231 cells were detached from cell culture plate surface using trypsin−EDTA (Gibco, USA). A droplet of cell suspension in DMEM was placed on CaF_2. To prevent any flow during the measurements, the cells were left to settle down on the CaF_2 surface for 5−10 min. An area was selected for the SERS acquisition. First, the system was calibrated by using a specific silicon which is Raman shift standard. The silicon gives a peak at 520 cm^{-1}. The spectra from the cell samples were collected using a Renishaw's Raman microscopy system with StreamLine. Laser power (150 mW) and exposure time (2 s) were preferred based on the optimizations done by Kuku et al.[21] A long distance 20× (N.A: 0.4) objective was used, and raster scans with 2 μm steps were done at 830 nm excitation wavelength. The step size was calculated using the spot size of laser beam on the sample surface, which was 2.5 μm according to the 1.22λ/NA formula. The spectra were acquired from 36 to 64 points per a single cell, and a total of 20 cells were used for analysis per combination of treatments. The measured spectra were processed using Wire software.

RESULTS AND DISCUSSION

Characterization of AuNPs. The absorption and scattering properties of AuNPs provide information about particle size and surface chemistry through their unique plasmonic properties. A schematic representation for the sizes and modification of the AuNPs is given in Figure S1. The UV/vis spectra of the $AuNPs_{13}$, $AuNPs_{13}$-oligo, $AuNPs_{50}$, and $AuNPs_{50}$-oligo are shown in Figure S2A. In agreement with the values reported in the literature, maximum wavelengths of the $AuNPs_{13}$ and $AuNPs_{50}$ were measured at 520 nm[48] and 532 nm[49], respectively. When the AuNPs were modified with oligonucleotides, maximum wavelength of $AuNPs_{13}$ shifted from 520 to 531 nm and the maximum wavelength of $AuNPs_{50}$ shifted from 532 to 540 nm. The observed band broadening and a shift about 10 nm in maximum absorption is the result of

DOI: 10.1021/acs.langmuir.8b03988
Langmuir 2019, 35, 4020−4028

both of the surface modification and aggregation of the NPs in colloidal suspension.[50]

Hydrodynamic size distributions of $AuNPs_{13}$, $AuNPs_{50}$, $AuNPs_{13}$-oligo, and $AuNPs_{50}$-oligo in their colloidal suspensions were also analyzed by using DLS. As shown in Figure S2B, when oligonucleotide was form a monolayer on their surfaces, the hydrodynamic size of $AuNPs_{13}$ and $AuNPs_{50}$, shifts from 13 to 28 nm and from 58 to 90 nm, respectively.

It is well known that when the AuNPs are suspended in the cell culture medium, serum proteins are nonspecifically adsorbed on the surface of AuNPs as they are uptaken by endocytosis. The adsorption of proteins associates with the size and surface chemistry of the nanoparticles. For the investigation of protein corona formation, the $AuNPs_{13}$, $AuNPs_{13}$-oligo, $AuNPs_{50}$, and their mixtures, $AuNPs_{50}$ + $AuNPs_{13}$ and $AuNPs_{50}$ + $AuNPs_{13}$-oligo were dispersed in the cell culture medium. The formation of corona and the interactions of AuNPs with different sizes and surface chemistries during the mixture of treatments and their aggregation were analyzed by monitoring the changes in time-dependent manner reflected on their absorption spectra and hydrodynamic sizes (Figure 1). It was found that protein corona formation caused the formation of large $AuNP_{13}$ aggregates as soon as AuNPs were added into the cell culture medium (Figure S3) as observed from a red shift to 555 nm from 520 nm in the UV/vis spectrum shown in Figure 1A. A broadening around 527 nm indicated the presence of different sizes of aggregates in the cell culture medium. The $AuNPs_{13}$-oligo showed an absorption spectrum similar to $AuNP_{13}$ upon their suspension in the cell culture medium. In the case of $AuNPs_{50}$, a red shift in the maximum absorbance was observed from 532 to 558 nm, also indicating the protein corona formation and aggregation. For the AuNP mixtures, a shift in the maximum absorption and broadening in the spectra were observed, indicating the protein corona formation and a weak interparticle interaction among the AuNPs in the $AuNPs_{50}$ + $AuNPs_{13}$ and $AuNPs_{50}$ + $AuNPs_{13}$-oligo mixtures.

Figure 1B, C shows the DLS spectra of the AuNPs in the cell culture medium. As it is seen on UV/vis spectra, the large intraparticle aggregates are formed and the hydrodynamic sizes of $AuNPs_{13}$ and $AuNP_{50}$ increase to 79 and 106 nm, respectively. When the mixture of $AuNPs_{13}$ + $AuNP_{50}$ is analyzed, a broad size distribution band with a maximum intensity at 68 nm is observed, which indicates weak interparticle interactions between $AuNPs_{13}$ and $AuNP_{50}$ and decreases the possibility of the formation of large intraparticle aggregate formation. The hydrodynamic size distribution in the case of the $AuNP_{13}$-oligo and the $AuNP_{50}$ + $AuNP_{13}$-oligo is given on Figure 1C. The oligonucleotide modification increases the hydrodynamic size of $AuNP_{13}$ to 122 nm. The hydrodynamic size distributions of AuNPs in the mixture are obtained smaller than that of the $AuNP_{50}$ and $AuNPs_{13}$-oligo, which may be because of a similar reason explained for the $AuNPs_{50}$ + $AuNPs_{13}$ mixture above.

Please note that the intracellular uptake of AuNPs is not only affected from the protein corona formation but also the size, which influences the wrapping of AuNPs into the cell. For example, small particles must be clustered to drive enough force, whereas 50 nm AuNPs induce enough energy for wrapping.[51,52] Thus, 50 nm AuNPs are more effectively uptaken by the cells.

TEM Image. Since endosomal trafficking is important in the metastasis of tumor cells and it can be a target for a treatment strategy, MDA-MB-231 metastatic breast cancer cells are used as a model cell line in this study.[53] Understanding the localization and aggregation of AuNPs[54] inside the cell would help to elucidate the spectral outcome about biochemical processes during endocytosis. Figure S4 is the TEM image of a cell treated with $AuNPs_{50}$ for 24 h. The figure shows that AuNP aggregates are present in the endosomal vesicles, whereas a lesser amount of AuNPs are located in cytoplasm individually. Figure 2 shows the TEM image of a MDA-MB-231 cell after incubation with the mixture of $AuNPs_{50}$-oligo and $AuNPs_{13}$ for 24 h. As seen, more than one AuNP aggregates were formed inside the cell. In Figure 2A, different aggregate compositions and shapes can be seen in the endosomal vesicles of a cell. In Figure 2B, the aggregates of $AuNPs_{50}$-oligo and the mixture of $AuNPs_{50}$-oligo and $AuNP_{13}$ can be seen in a tightly packed rod shape. In Figure 2C, a larger $AuNP_{13}$ aggregate with a few $AuNPs_{50}$-oligo in between can be seen in a less compact shape.

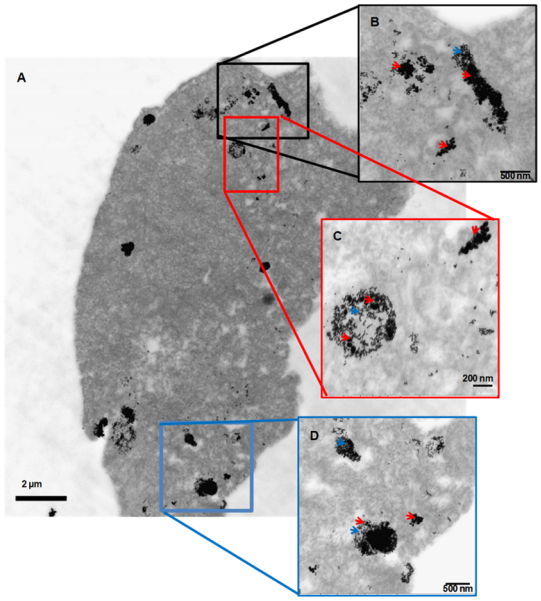

Figure 2. TEM images of (A) AuNP aggregates in a single MDA-MB-231 cell treated with a mixture of 25 nM of $AuNPs_{50}$-oligo and 10 nm of $AuNPs_{13}$ for 24 h and (B–D) magnifications of AuNP aggregates.

In Figure 2D, a tightly packed spherical-shaped $AuNPs_{50}$-oligo and $AuNP_{13}$ mixture is seen, suggesting that the AuNP aggregates are formed with random ratios and compositions in the endosomes when they are added together. The random nanoparticle ratios in endolysosomes can be explained with two scenarios. In the first scenario, as it was observed in UV/vis and DLS study (Figure 1), the AuNPs in mixtures can adhere each other through weak interactions when they are introduced into the cell culture medium increasing the possibility of uptake together. In the second scenario, the mature vesicular buds contain AuNPs with different sizes travel and fuse into large endolysosomes forming random nanoparticle aggregate compositions. It is also possible that both scenarios take place at the same time.

Time-Dependent SERS Activity on AuNPs. Because of the induced different molecular dynamics of cells during $AuNPs_{50}$, $AuNPs_{50}$-oligo, mixtures of $AuNPs_{50}$/$AuNPs_{13}$, and $AuNPs_{50}$/$AuNPs_{13}$-oligo treatments, significant changes in intensities of SERS signals were clearly observed over time.

DOI: 10.1021/acs.langmuir.8b03988
Langmuir 2019, 35, 4020–4028

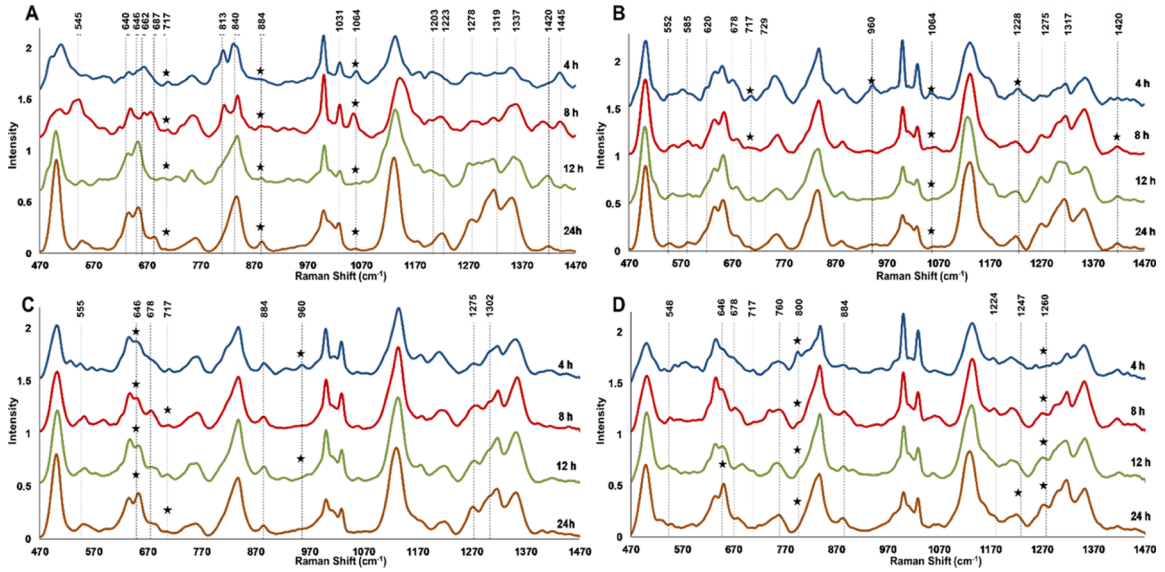

Figure 3. Comparison of SERS spectra from MDA-MB231 cells incubated with (A) $AuNPs_{50}$, (B) $AuNPs_{50}$-oligo, (C) $AuNPs_{50}$ and $AuNPs_{13}$, and (D) $AuNPs_{50}$ and $AuNPs_{13}$-oligo for 4, 8, 12, and 24 h. The average spectra from 20 single cells were used for analysis.

Please note that AuNPs are known to be nontoxic.[35] However, toxicity of AuNPs can change depending on surface chemistry, shape, size, and aggregation status[55] Therefore, in order to be sure that the spectral changes were not caused by the cytotoxicity of AuNPs, the effects of $AuNPs_{13}$, $AuNPs_{13}$-oligo, $AuNPs_{50}$, $AuNPs_{50}$-oligo, mixture of $AuNPs_{50}$ + $AuNPs_{13}$, and mixture of $AuNPs_{50}$ + $AuNPs_{13}$-oligo on the cell viability were first investigated. As seen in Figure S5, the AuNPs were not toxic at concentration in which the SERS analysis was performed.

After validating the nontoxicity, cells were incubated with AuNPs and the cellular responses were investigated with SERS. As it was demonstrated in Figure 2, AuNPs were aggregated in endosomes. The endocytotic pathway of the AuNPs was previously explained by Kneipp et al.[41] Briefly, AuNPs are taken up by the early endosomes with the help of cargo proteins and lipids. Vesicular bud matures and can undergo fusion with endolysosomes, forming dimers and trimers of the AuNPs. Meanwhile, proteins and receptors play a major role during these processes especially cysteine-rich proteins.[56] As the incubation duration increases, particles form larger aggregates. The changes in biochemical processes in endosomal vesicles can be seen on the SERS spectra over incubation period in Figure 3. The obtained spectral changes are possibly due to endosome maturation and the aggregation status of AuNPs.

The spectral changes during $AuNPs_{50}$ treatment from 4 to 24 h are shown in Figure 3A. The summary of tentative peak assignments is given in Table S1. As seen, the intensities corresponding to proteins, amino acids, and nucleic acids increase starting from 4 to 24 h, whereas the intensity of the peaks pertaining to lipids decreases. These spectral changes are observed because of the endosomal dynamic changes due to the aggregation status of $AuNPs_{50}$ in the cell over time. For example, when the intensity of the C−N bond in membrane phospholipids (717 cm^{-1}) decreased, the peak intensity of proteins at 884 cm^{-1} increased over exposure time.

After 8 h, the peaks corresponding to S−S and C−C bonds of proteins between 500 and 600 cm^{-1} could be clearly observed,[57] indicating the formation of endolysosomes. After 12 h, peak intensities, which correspond to proteins and nucleic acids (1200 and 1400 cm^{-1}), started to increase as the exposure time increases. This can be explained by the formation of larger aggregates of AuNPs inside endolysosome, which might cause increased GTPase activity to provide sufficient energy needed for the regulation of endolysosomal protein structure.[58] After 12 h, the peak at 813 cm^{-1} that corresponds to phosphodiester bond disappeared.

Besides these, the amide III bonds in the range of 1200−1400 cm^{-1}, which give structural information about the proteins, increased, demonstrating the changes of protein structures in the endosomes over time. Decreases in the C−C stretch (1064 cm^{-1}) and CH_2 deformation (1445 cm^{-1}), which are associated with endosomal membrane status of lipids, are observed. All of these spectral changes indicate that the interaction of $AuNPs_{50}$ with endosomal membrane decreased with the maturation from early endosome to late endosomes.

In the case of $AuNPs_{50}$-oligo treatment, intensities which correspond to nucleic acids and proteins increased; and the peaks which correspond to lipids also decreased during the exposure time. The peak at 1228 cm^{-1}, which corresponds to amide III, sharpened with increased exposure time. In addition, the peaks between 1200 and 1400 cm^{-1} increased. Spectral changes were also observed between 500 and 600 cm^{-1} which correspond to the S−S bond.

More specifically, after 4 h, there were significant decreases at 960 and 1064 cm^{-1} which correspond to PO_4^{3-} and C−C in lipids, respectively. In addition, the peak at 1420 cm^{-1}, which is attributed to nucleic acids, showed up after 8 h. The peak intensity at 717 cm^{-1}, which corresponds to the C−N bond in the membrane phospholipids, decreased between 8 and 24 h treatment. As expected, the spectral changes which correspond to protein, lipids, and nucleic acids were observed. Generally, the intensities of protein and nucleic acid peaks increased, and the lipid peaks decreased as the exposure time increased.

As mentioned before, the nanoparticle uptake and intracellular aggregation status are influenced by the size and surface chemistry of nanoparticles.[37] In this study, we have also investigated the effects of uptake and intracellular aggregation

DOI: 10.1021/acs.langmuir.8b03988
Langmuir 2019, 35, 4020−4028

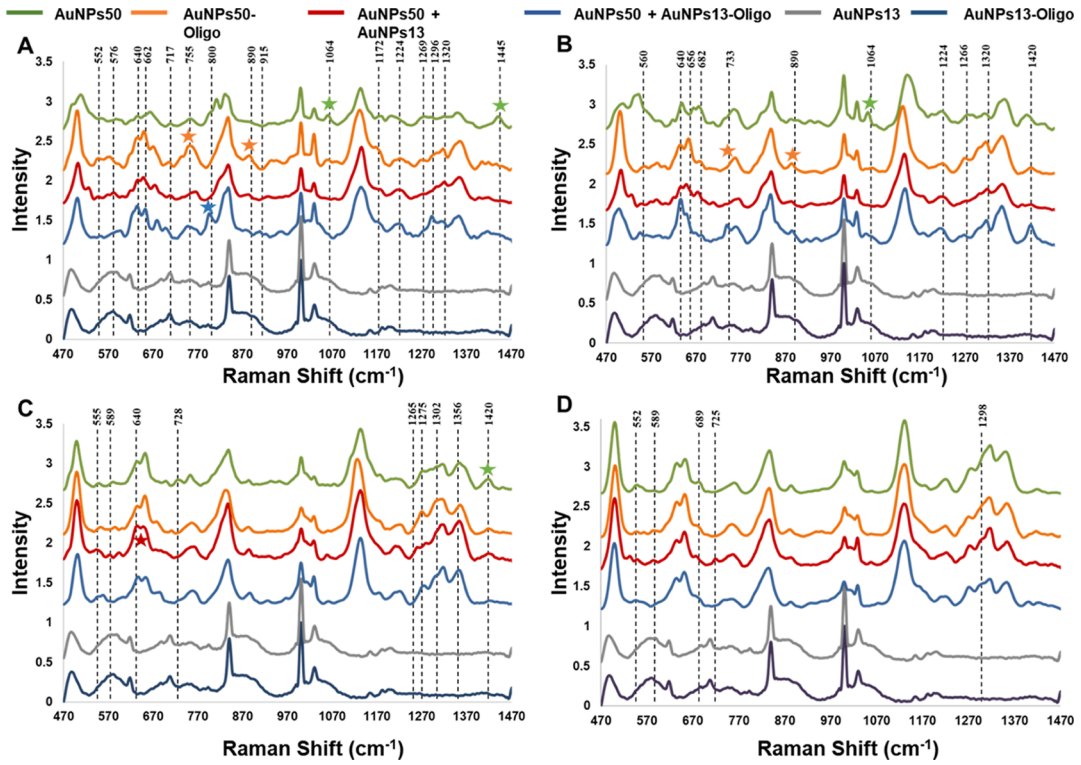

Figure 4. SERS spectra of MDA-MB-231 cells incubated with $AuNPs_{13}$, $AuNPs_{13}$-oligo, $AuNPs_{50}$, $AuNPs_{50}$-oligo, $AuNPs_{50}$ + $AuNPs_{13}$, and $AuNPs_{50}$ + $AuNPs_{13}$-oligo for (A) 4, (B) 8, (C) 12, and (D) 24 h. The average spectra from 20 single cells were used for analysis.

of different sizes and surface chemistries when they are exposed together on SERS spectra. We used a mixture of $AuNPs_{50}$ and $AuNPs_{13}$ and $AuNPs_{50}$ and $AuNPs_{13}$-oligo for the investigation.

Time-dependent SERS activity was monitored after 4, 8, 12, and 24 h treatments with a mixture of $AuNPs_{50}$ and $AuNPs_{13}$. As seen in Figure 3C, after 4 and 8 h treatments, spectral changes corresponding to the S−S bond (500−600 cm^{-1}) are observed. These spectral changes can be explained as the formation of endolysosome in the cells in which cystein-rich proteins play a role.[56] Again, in this case, as the exposure time increased, protein peaks increased and lipid peaks decreased. For example, the peak intensity at 646 cm^{-1} (C−C twisting mode of tyrosine) increased significantly, whereas the peak intensities at 717 and 960 cm^{-1} corresponding to C−N and PO_4^{3-} in lipids, respectively, disappeared after 24 h.

The mixture of $AuNPs_{50}$ and $AuNPs_{13}$-oligo was also used to investigate the effects of surface chemistry on SERS spectra. As similar to the other treatments, protein peaks increased and lipid peaks decreased over 24 h. For example, after 24 h, the peak corresponding to the C−C twisting mode of tyrosine (646 cm^{-1}) significantly increased, whereas the peak corresponding to PO_4^{3-} interactions (800 cm^{-1}) significantly decreased. Also, 1224, 1247, and 1260 cm^{-1} peaks corresponding to amide III bonds increased during 24 h as well. We can say that SERS analysis is so sensitive to show surface chemistry-dependent biochemical changes on the spectral outcome. The spectral changes corresponding to proteins and lipids were clearly observed during $AuNPs_{50}$ and $AuNPs_{13}$-oligo mixture treatment. Note that we cannot observe the spectra from the oligonucleotide attached on $AuNPs_{13}$ (Figure S6). The observed spectral changes were dominated by the biochemical changes in endosomal vesicles.

Substrate-Dependent SERS Activity on AuNPs. In this part of the study, the SERS spectra were analyzed at the same exposure times and compared with each case of AuNP treatments. The spectral changes of the cells treated for 4, 8, 12, and 24 h are shown in Figure 4. Because the first step of endocytosis is the membrane wrapping and vesicle forming, we expected spectral changes corresponding to lipids and proteins, especially in the first 4 h. In the case of $AuNPs_{50}$, the SERS spectra dominated by membrane lipids as observed from the spectral changes corresponding to CH_2 deformation and C−C bond in lipids (1064 and 1445 cm^{-1}, respectively). However, after $AuNPs_{50}$-oligo treatments, the peaks at proteins and amide III (640, 662, and 755, 1200−1400 cm^{-1}) increased because proteins play an important role in the formation of vesicles. In addition, the nucleic acids and proteins peaks (552, 800, 890, and 1172 cm^{-1}) were just observed for $AuNPs_{50}$-oligo. Thus, we can conclude that the endosomal vesicles started to be formed more rapidly during $AuNPs_{50}$-oligo treatment compared to $AuNPs_{50}$ treatment at 4 h. We also see similar changes under $AuNPs_{50}$ + $AuNPs_{13}$-oligo mixture treatment, whereas it was not observed after $AuNPs_{50}$ + $AuNPs_{13}$ treatment. Thus, it can be said that oligonucleotide modification on the AuNP surface can accelerate the endocytic process and cellular uptake by the help of proteins adsorbed on oligonucleotide-modified AuNPs, which decrease the decelerating effect of thick protein corona adsorbed nonspecifically on the surface. The interaction of these nanoparticles with the receptors should have an impact to induce enough energy to wrap nanoparticles.[59−62]

Spectral changes, especially corresponding to proteins and nucleic acids (500−600 cm^{-1}), are observed after 8 h treatment. This can be explained with the formation of late endosomes because multivesicular bodies may be formed by

DOI: 10.1021/acs.langmuir.8b03988
Langmuir 2019, 35, 4020−4028

the endosomes after 8 h. However, the only lipid peak at 1064 cm^{-1} was observed for $AuNPs_{50}$ treatment after 8 h. It could be explained as the localization of aggregation of $AuNPs_{50}$, as $AuNPs_{50}$ still could have remained close to the membrane at 8 h.

It is difficult to correlate the observed spectral changes with the the molecular basis of transport. However, a peak at 733 cm^{-1}, attributed to phosphatidylserine, was observed with the $AuNPs_{50}$ + $AuNPs_{13}$-oligo mixture treatment could be due to the endosomal vesicle transport facilitated by adenosine triphosphate (ATP) enhanced phospharidylserine flipping.

In addition, the increase in the intensity of the protein peak at 890 cm^{-1} after 8 h of $AuNPs_{50}$-oligo and $AuNPs_{50}$ + $AuNPs_{13}$-oligo mixture treatments as a result of the rapid endosomal maturation indicates that the oligonucleotide coating on the surfaces of AuNPs facilitate the cellular uptake.

After 12 h treatment, the number of spectral changes decreased. The spectral changes corresponding to S−S and C−C bonds in proteins (555, 589, 640, and 728 cm^{-1}, respectively) are observed for all AuNP treatments. With the $AuNPs_{50}$ treatment, a peak at 1420 cm^{-1} attributed to $-COO^-$ group of proteins appears as a result of better adsorption of proteins and peptides onto gold surfaces when pH is in the range of 6.2−6.9. However, this situation can be observed during early endosome or before the late endosome.[61] Although not yet certain, $AuNPs_{50}$ could still have remained at early endosomes or near the cell membrane after 12 h. This inference can be supported by protein corona formation data because $AuNPs_{50}$ had the highest rate of protein corona formation which leads to the faster decrease rate in the internalization of AuNPs.[50,56]

Finally, when cells were treated for 24 h, the number of spectral changes between AuNP treatments decreased significantly. This is expected because the uptake of AuNPs should be almost completed after 24 h. Yet, the spectral changes between 552 and 725 cm^{-1}, which correspond to adenine and phosphate groups, could be observed because of the acidification with V-ATPases as a result of endolysosomes formation.[62]

CONCLUSIONS

SERS is a promising technique for single-cell analysis. When interpreting the SERS spectra, cellular uptake processes of AuNPs should be carefully considered. Because the uptake of AuNPs is a dynamic process, their aggregation status continuously changes until they settle down in the hybrid structure, endolysosome. During the uptake process, proteins and cell surface receptors play very important roles. This could be one of the factors influencing the observed spectral variation, which can be traced to monitor biomolecular processes in a single cell. In our study, we demonstrated the use of SERS as a possible nanosensing tool for biochemical processes in a single cell based on investigations of the different sizes, surface chemistries, and incubation times for AuNPs. The investigations using $AuNPs_{50}$, $AuNPs_{50}$-oligo, mixture of $AuNPs_{50}$ and $AuNPs_{13}$, and mixture of $AuNPs_{50}$ and $AuNPs_{13}$-oligo demonstrated the importance of the AuNP size and surface properties on SERS activity.

The spectral changes were observed with endosomal activity such as vesicle formation, motion, and endosome−lysosome fusion. The increase in the peak intensities corresponding to protein structures and the decrease in the peak intensities of phospholipid structures could be used for the monitoring of maturation of endosomes from early endosome to endolysosomes.

The time-dependent analysis observed in the SERS spectra demonstrated that the oligonucleotide surface chemistry strongly influenced the wrapping of AuNPs and their aggregation status at the initial incubation times, possibly through the protein corona status on the AuNPs during the first 8 h. After 24 h, as AuNPs settled down in the fused endosome−lysosome hybrid structures, the spectral variation decreased.

In conclusion, this study shows that the size, surface chemistry, and aggregation status of the AuNPs play important roles in deciding their endosomal route and this can be observed from SERS spectral changes as the endosome evolves. Because AuNPs are one of the promising materials for drug or gene delivery application, tracing the endosomal activity during their uptake may inform us about their performance. In future, the use of similar approaches with different cell lines would add invaluable insight into the nature of the endocytosis process taking place on the AuNP surfaces as they travel into the cells.

ASSOCIATED CONTENT

Supporting Information

The Supporting Information is available free of charge on the ACS Publications website at DOI: 10.1021/acs.langmuir.8b03988.

Schematic representation of sizes, modifications, and interaction of AuNPs with the molecules at different endosomal stages, UV/vis and DLS of AuNPs, TEM image of $AuNP_{50}$ in endosomes, cell viability analysis, SERS spectra of cells treated with $AuNPs_{13}$ and $AuNPs_{13}$-oligo, experimental setup, and tentative SERS spectra assignments (PDF)

AUTHOR INFORMATION

Corresponding Author

*E-mail: mculha@yeditepe.edu.tr. Phone: +90 (216) 578 1587. Fax: +90 (216) 578 0829.

ORCID

Mustafa Çulha: 0000-0002-3844-5190

Notes

The authors declare no competing financial interest.

ACKNOWLEDGMENTS

The authors acknowledge the financial support from Yeditepe University. We would like to thank Melike Sarıçam for her help during the modification of AuNPs with oligonucleotides.

REFERENCES

(1) Lodish, H.; Berk, A.; Kaiser, C.; Krieger, M.; Bretscher, A.; Ploegh, H.; Amon, A.; Scott, M. Transmembrane transport of ions and small molecules. In *Molecular Cell Biology*, 7th ed.; W.H. Freeman & Company: New York, 2012; pp 473−516.

(2) Kleinman, S. L.; Frontiera, R. R.; Henry, A.-I.; Dieringer, J. A.; Van Duyne, R. P. Creating, characterizing, and controlling chemistry with SERS hot spots. *Phys. Chem. Chem. Phys.* **2013**, *15*, 21−36.

(3) Olive, P. L.; Banáth, J. P.; Durand, R. E.; Banath, J. P. Heterogeneity in Radiation-Induced DNA Damage and Repair in Tumor and Normal Cells Measured Using the "Comet" Assay. *Radiat. Res.* **1990**, *122*, 86−94.

(4) Zhang, L.; Cui, X.; Schmitt, K.; Hubert, R.; Navidi, W.; Arnheim, N. Whole genome amplification from a single cell: implications for genetic analysis. *Proc. Natl. Acad. Sci. U.S.A.* **1992**, *89*, 5847−5851.

DOI: 10.1021/acs.langmuir.8b03988
Langmuir 2019, 35, 4020−4028

(5) StÅhlberg, A.; Kubista, M. The workflow of single-cell expression profiling using quantitative real-time PCR. *Expert Rev. Mol. Diagn.* **2014**, *14*, 323−331.
(6) Müller, S.; Nebe-von-Caron, G. Functional single-cell analyses: flow cytometry and cell sorting of microbial populations and communities. *FEMS Microbiol. Rev.* **2010**, *34*, 554−587.
(7) Angelo, M.; Bendall, S. C.; Finck, R.; Hale, M. B.; Hitzman, C.; Borowsky, A. D.; Levenson, R. M.; Lowe, J. B.; Liu, S. D.; Zhao, S.; Natkunam, Y.; Nolan, G. P. Multiplexed ion beam imaging of human breast tumors. *Nat. Med.* **2014**, *20*, 436−442.
(8) Kim, K. S.; Cho, C. H.; Park, E. K.; Jung, M.-H.; Yoon, K.-S.; Park, H.-K. AFM-detected apoptotic changes in morphology and biophysical property caused by paclitaxel in Ishikawa and HeLa cells. *PLoS One* **2012**, *7*, No. e30066.
(9) Henriques, R.; Griffiths, C.; Hesper Rego, E.; Mhlanga, M. M. PALM and STORM: Unlocking live-cell super-resolution. *Biopolymers* **2011**, *95*, 322−331.
(10) Puppels, G. J.; De Mul, F. F. M.; Otto, C.; Greve, J.; Robert-Nicoud, M.; Arndt-Jovin, D. J.; Jovin, T. M. Studying single living cells and chromosomes by confocal Raman microspectroscopy. *Nature* **1990**, *347*, 301.
(11) Palonpon, A. F.; Sodeoka, M.; Fujita, K. Molecular imaging of live cells by Raman microscopy. *Curr. Opin. Chem. Biol.* **2013**, *17*, 708−715.
(12) Howat, W. J.; Wilson, B. A. Tissue fixation and the effect of molecular fixatives on downstream staining procedures. *Methods* **2014**, *70*, 12−19.
(13) Chan, J. W.; Taylor, D. S.; Thompson, D. L. The effect of cell fixation on the discrimination of normal and leukemia cells with laser tweezers Raman spectroscopy. *Biopolymers* **2009**, *91*, 132−139.
(14) Schie, I. W.; Alber, L.; Gryshuk, A. L.; Chan, J. W. Investigating drug induced changes in single, living lymphocytes based on Raman micro-spectroscopy. *Analyst* **2014**, *139*, 2726−2733.
(15) Konorov, S. O.; Schulze, H. G.; Piret, J. M.; Blades, M. W.; Turner, R. F. B. Label-free determination of the cell cycle phase in human embryonic stem cells by Raman microspectroscopy. *Anal. Chem.* **2013**, *85*, 8996−9002.
(16) Smith, E.; Dent, G. *Modern Raman Spectroscopy: A Practical Approach*; John Wiley & Sons, 2013.
(17) Jeanmaire, D. L.; Van Duyne, R. P. Surface Raman spectroelectrochemistry: Part I. Heterocyclic, aromatic, and aliphatic amines adsorbed on the anodized silver electrode. *J. Electroanal. Chem. Interfacial Electrochem.* **1977**, *84*, 1−20.
(18) Nabiev, I.; Morjani, H.; Manfait, M. Selective analysis of antitumor drug interaction with living cancer cells as probed by surface-enhanced Raman spectroscopy. *Eur. Biophys. J.* **1991**, *19*, 311−316.
(19) Zhang, Q.; Lu, X.; Tang, P.; Zhang, D.; Tian, J.; Zhong, L. Gold Nanoparticle (AuNP)-Based Surface-Enhanced Raman Scattering (SERS) Probe of Leukemic Lymphocytes. *Plasmonics* **2016**, *11*, 1361−1368.
(20) Xu, L.; Kuang, H.; Xu, C.; Ma, W.; Wang, L.; Kotov, N. A. Regiospecific plasmonic assemblies for in situ Raman spectroscopy in live cells. *J. Am. Chem. Soc.* **2012**, *134*, 1699−1709.
(21) Kuku, G.; Saricam, M.; Akhatova, F.; Danilushkina, A.; Fakhrullin, R.; Culha, M. Surface-enhanced Raman scattering to evaluate nanomaterial cytotoxicity on living cells. *Anal. Chem.* **2016**, *88*, 9813−9820.
(22) Kim, T.-H.; Lee, K.-B.; Choi, J.-W. 3D graphene oxide-encapsulated gold nanoparticles to detect neural stem cell differentiation. *Biomaterials* **2013**, *34*, 8660−8670.
(23) El-Said, W. A.; Kim, S. U.; Choi, J.-W. Monitoring in vitro neural stem cell differentiation based on surface-enhanced Raman spectroscopy using a gold nanostar array. *J. Mater. Chem. C* **2015**, *3*, 3848−3859.
(24) Campion, A.; Kambhampati, P. Surface-enhanced Raman scattering. *Chem. Soc. Rev.* **1998**, *27*, 241−250.
(25) Lee, P. C.; Meisel, D. Adsorption and surface-enhanced Raman of dyes on silver and gold sols. *J. Phys. Chem.* **1982**, *86*, 3391−3395.
(26) Mikoliunaite, L.; Rodriguez, R. D.; Sheremet, E.; Kolchuzhin, V.; Mehner, J.; Ramanavicius, A.; Zahn, D. R. The substrate matters in the Raman spectroscopy analysis of cells. *Sci. Rep.* **2015**, *5*, 13150.
(27) Jiang, X.; Jiang, Z.; Xu, T.; Su, S.; Zhong, Y.; Peng, F.; Su, Y.; He, Y. Surface-enhanced Raman scattering-based sensing in vitro: facile and label-free detection of apoptotic cells at the single-cell level. *Anal. Chem.* **2013**, *85*, 2809−2816.
(28) El-Said, W. A.; Kim, T.-H.; Kim, H.; Choi, J.-W. Analysis of intracellular state based on controlled 3D nanostructures mediated surface enhanced Raman scattering. *PLoS One* **2011**, *6*, No. e15836.
(29) Jin, Q.; Li, M.; Polat, B.; Paidi, S. K.; Dai, A.; Zhang, A.; Pagaduan, J. V.; Barman, I.; Gracias, D. H. Mechanical Trap Surface-Enhanced Raman Spectroscopy for Three-Dimensional Surface Molecular Imaging of Single Live Cells. *Angew. Chem.* **2017**, *129*, 3880−3884.
(30) Vitol, E. A.; Orynbayeva, Z.; Bouchard, M. J.; Azizkhan-Clifford, J.; Friedman, G.; Gogotsi, Y. In situ intracellular spectroscopy with surface enhanced Raman spectroscopy (SERS)-enabled nanopipettes. *ACS Nano* **2009**, *3*, 3529−3536.
(31) Huang, J.-Y.; Zong, C.; Xu, L.-J.; Cui, Y.; Ren, B. Clean and modified substrates for direct detection of living cells by surface-enhanced Raman spectroscopy. *Chem. Commun.* **2011**, *47*, 5738−5740.
(32) Yu, Y.; Wang, J.; Lin, J.; Lin, D.; Chen, W.; Feng, S.; Huang, Z.; Li, Y.; Huang, H.; Shi, H.; Chen, R. An optimized electroporation method for delivering nanoparticles into living cells for surface-enhanced Raman scattering imaging. *Appl. Phys. Lett.* **2016**, *108*, 153701.
(33) Lévy, R.; Shaheen, U.; Cesbron, Y.; Sée, V. Gold nanoparticles delivery in mammalian live cells: a critical review. *Nano Rev.* **2010**, *1*, 4889.
(34) Shamsaie, A.; Jonczyk, M.; Sturgis, J.; Paul Robinson, J.; Irudayaraj, J. Intracellularly grown gold nanoparticles as potential surface-enhanced Raman scattering probes. *J. Biomed. Optic.* **2007**, *12*, 020502.
(35) Connor, E. E.; Mwamuka, J.; Gole, A.; Murphy, C. J.; Wyatt, M. D. Gold nanoparticles are taken up by human cells but do not cause acute cytotoxicity. *Small* **2005**, *1*, 325−327.
(36) Rejman, J.; Oberle, V.; Zuhorn, I. S.; Hoekstra, D. Size-dependent internalization of particles via the pathways of clathrin- and caveolae-mediated endocytosis. *Biochem. J.* **2004**, *377*, 159−169.
(37) Ma, N.; Ma, C.; Li, C.; Wang, T.; Tang, Y.; Wang, H.; Mou, X.; Chen, Z.; He, N. Influence of nanoparticle shape, size, and surface functionalization on cellular uptake. *J. Nanosci. Nanotechnol.* **2013**, *13*, 6485−6498.
(38) Kneipp, K.; Wang, Y.; Kneipp, H.; Perelman, L. T.; Itzkan, I.; Dasari, R. R.; Feld, M. S. Single molecule detection using surface-enhanced Raman scattering (SERS). *Phys. Rev. Lett.* **1997**, *78*, 1667.
(39) Altunbek, M.; Kuku, G.; Culha, M. Gold nanoparticles in single-cell analysis for surface enhanced Raman scattering. *Molecules* **2016**, *21*, 1617.
(40) Kneipp, K.; Haka, A. S.; Kneipp, H.; Badizadegan, K.; Yoshizawa, N.; Boone, C.; Shafer-Peltier, K. E.; Motz, J. T.; Dasari, R. R.; Feld, M. S. Surface-enhanced Raman spectroscopy in single living cells using gold nanoparticles. *Appl. Spectrosc.* **2002**, *56*, 150−154.
(41) Kneipp, J.; Kneipp, H.; McLaughlin, M.; Brown, D.; Kneipp, K. In vivo molecular probing of cellular compartments with gold nanoparticles and nanoaggregates. *Nano Lett.* **2006**, *6*, 2225−2231.
(42) Huefner, A.; Kuan, W.-L.; Müller, K. H.; Skepper, J. N.; Barker, R. A.; Mahajan, S. Characterization and visualization of vesicles in the endo-lysosomal pathway with surface-enhanced Raman spectroscopy and chemometrics. *ACS Nano* **2015**, *10*, 307−316.
(43) Büchner, T.; Drescher, D.; Merk, V.; Traub, H.; Guttmann, P.; Werner, S.; Jakubowski, N.; Schneider, G.; Kneipp, J. Biomolecular environment, quantification, and intracellular interaction of multifunctional magnetic SERS nanoprobes. *Analyst* **2016**, *141*, 5096−5106.

DOI: 10.1021/acs.langmuir.8b03988
Langmuir 2019, 35, 4020−4028

(44) Taylor, J.; Milton, J.; Willett, M.; Wingfield, J.; Mahajan, S. What do we actually see in intracellular SERS? Investigating nanosensor-induced variation. *Faraday Discuss* **2017**, *205*, 409−428.
(45) Zhang, X.-Q.; Xu, X.; Lam, R.; Giljohann, D.; Ho, D.; Mirkin, C. A. Strategy for Increasing Drug Solubility and Efficacy through Covalent Attachment to Polyvalent DNA-Nanoparticle Conjugates. *ACS Nano* **2011**, *5*, 6962−6970.
(46) Enustun, B. V.; Turkevich, J. Coagulation of colloidal gold. *J. Am. Chem. Soc.* **1963**, *85*, 3317−3328.
(47) Mirkin, C. A.; Letsinger, R. L.; Mucic, R. C.; Storhoff, J. J. A DNA-based method for rationally assembling nanoparticles into macroscopic materials. *Nature* **1996**, *382*, 607.
(48) Murdock, R. C.; Braydich-Stolle, L.; Schrand, A. M.; Schlager, J. J.; Hussain, S. M. Characterization of nanomaterial dispersion in solution prior to in vitro exposure using dynamic light scattering technique. *Toxicol. Sci.* **2008**, *101*, 239−253.
(49) Abdelhalim, M. A. K.; Mady, M. M.; Ghannam, M. M. Physical properties of different gold nanoparticles: ultraviolet-visible and fluorescence measurements. *J. Nanomed. Nanotechnol.* **2012**, *3*, 133.
(50) Polavarapu, L.; Pérez-Juste, J.; Xu, Q.-H.; Liz-Marzán, L. M. Optical sensing of biological, chemical and ionic species through aggregation of plasmonic nanoparticles. *J. Mater. Chem. C* **2014**, *2*, 7460−7476.
(51) Chithrani, B. D.; Ghazani, A. A.; Chan, W. C. W. Determining the size and shape dependence of gold nanoparticle uptake into mammalian cells. *Nano Lett.* **2006**, *6*, 662−668.
(52) Yao, M.; He, L.; McClements, D. J.; Xiao, H. Uptake of gold nanoparticles by intestinal epithelial cells: impact of particle size on their absorption, accumulation, and toxicity. *J. Agric. Food Chem.* **2015**, *63*, 8044−8049.
(53) Mellman, I.; Yarden, Y. Endocytosis and cancer. *Cold Spring Harbor Perspect. Biol.* **2013**, *5*, a016949.
(54) Ding, Y.; Jiang, Z.; Saha, K.; Kim, C. S.; Kim, S. T.; Landis, R. F.; Rotello, V. M. Gold nanoparticles for nucleic acid delivery. *Mol. Ther.* **2014**, *22*, 1075−1083.
(55) Pan, Y.; Leifert, A.; Ruau, D.; Neuss, S.; Bornemann, J.; Schmid, G.; Brandau, W.; Simon, U.; Jahnen-Dechent, W. Gold nanoparticles of diameter 1.4 nm trigger necrosis by oxidative stress and mitochondrial damage. *Small* **2009**, *5*, 2067−2076.
(56) Scott, C. C.; Vacca, F.; Gruenberg, J. Endosome maturation, transport and functions. *Seminars in Cell & Developmental Biology*; Elsevier, 2014; pp 2−10.
(57) Austin, L. A.; Kang, B.; El-Sayed, M. A. A new nanotechnology technique for determining drug efficacy using targeted plasmonically enhanced single cell imaging spectroscopy. *J. Am. Chem. Soc.* **2013**, *135*, 4688−4691.
(58) Guerra, F.; Bucci, C. Multiple roles of the small GTPase Rab7. *Cells* **2016**, *5*, 34.
(59) Brodin, L.; Löw, P.; Shupliakov, O. Sequential steps in clathrin-mediated synaptic vesicle endocytosis. *Curr. Opin. Neurobiol.* **2000**, *10*, 312−320.
(60) Granger, E.; McNee, G.; Allan, V.; Woodman, P. The role of the cytoskeleton and molecular motors in endosomal dynamics. *Seminars in Cell & Developmental Biology*; Elsevier, 2014; Vol. *31*, pp 20−9.
(61) Kneipp, J.; Kneipp, H.; Wittig, B.; Kneipp, K. Following the dynamics of pH in endosomes of live cells with SERS nanosensors. *J. Phys. Chem. C* **2010**, *114*, 7421−7426.
(62) Huotari, J.; Helenius, A. Endosome maturation. *EMBO J.* **2011**, *30*, 3481−3500.

DOI: 10.1021/acs.langmuir.8b03988
Langmuir 2019, 35, 4020−4028